Effect of sputtering on self-damaged recrystallized W mirror specimens

V.S. Voitsenya[1], M. Balden[2], A.I. Belyaeva[3], V.Kh. Alimov[4], B. Tyburska-Püschel[2], A.A. Galuza[5], A.A. Kasilov[1], I.V. Kolenov[3], V.G. Konovalov[1], O.O. Skoryk[1], S.I. Solodovchenko[1]

[1]Institute of Plasma Physics, National Scientific Center ‘‘KIPT”, 61108 Kharkov, Ukraine
[2]Max-Planck-Institut für Plasmaphysik, EURATOM Association, D-85748 Garching, Germany
[3]National Technical University “Kharkiv Polytechnical Institute”, 61002 Kharkov, Ukraine
[4]Hydrogen Isotope Research Center, University of Toyama, Toyama 930-8555, Japan
[5]Institute of Electrophysics and Radiation Technologies, NAS of Ukraine, 61002 Kharkov, Ukraine

Abstract The effect of heavy sputtering and of neutron irradiation simulated by displacement damaging with of 20 MeV W^{6+} ions on the optical properties of tungsten mirrors was studied. Ar^+ ions with 600 eV of energy were used as imitation of charge exchange atoms ejected from fusion plasma. The ion fluence dependence of the surface topography and the optical properties of polycrystalline, recrystallized tungsten (grain size 20 - 100 μm) were studied by optical microscopy, interferometry, reflectrometry and ellipsometry. Furthermore, after sputtering in total a layer of 3.9 μm in thickness, the orientation and the thickness of the eroded layer of many individual grains was determined by electron backscattering diffraction and confocal laser scanning microscopy. Concluding from the obtained data the neutron irradiation, at least at the damage level would be achieved in ITER, has not to make an additional contribution in the processes developing under impact of charge exchange atoms only.

1. Introduction

Optical diagnostics are an essential part of diagnostic systems of current and future fusion devices. In ITER all optical measurements have to be based on reflective optics. The most crucial of these systems will be the first mirrors (FM) which are plasma-facing components of diagnostic schemes. The main criterion to the FM materials is high reflecting ability together with resistance to radiation damages due to impact of 14 MeV neutrons from the D–T fusion reaction and charge exchange atoms (CXA). Simultaneous impact of the neutrons and CXA can promote faster degradation of optical properties of the mirror in comparison with the impact of CXA only. Defects created by the neutrons in the near-surface layer can be a reason of faster change of surface morphology, and correspondingly, faster degradation of optical properties under impact of CXA flux.

Previously such effect was examined for copper and stainless steel mirrors [1, 2] irradiated with high energy (1-3 MeV) Cu^+ and Cr^+ ions for simulating neutron irradiation. It was found that degradation of these mirrors under long term sputtering with hydrogen plasma occurs with approximately similar rate as that for the mirrors not preliminary bombarded with high energy metal ions.

This result allows a conclusion that simultaneous irradiation with neutrons and CXA does not result in significant increase of rate of degradation of optical properties of metallic mirrors compared to irradiation with CXA only.

However, above-mentioned experiments were carried out with metals which will not be used in ITER as the plasma-facing components [3]. Thus, there is an interest to perform similar

comparative experiments with tungsten, which was chosen to be one of the plasma facing materials of in-vessel components of the ITER construction [3].

In addition, there is a quite high probability that just tungsten will be a priority material for fabrication of FMs located in positions where they will be subjected to strong sputter erosion, as follows from the so-called R/Y criterion, where R is the reflectance, Y is the sputtering yield. This criterion was suggested [4] to choose FM materials disposed in erosion-dominating areas of first wall and divertor. The R/Y criterion shown in Table 1 for selected materials indicates evidentially that tungsten is favorable materials for areas where sputtering rate is high.

Below we present and discuss results obtained with recrystallized tungsten specimens preliminary irradiated with 20 MeV tungsten ions and then subjected to a long term sputtering with Ar ions.

2. Experiment

Recrystallized tungsten (rc W) was used in this work. The tungsten plate with purity of 99.99 wt% and with 99.7% of theoretical density was prepared (A.L.M.T. Corp., Japan) by powder metallurgy and hot-rolled reduction [5, 6]. The plate was cut into specimens of 10×10×2 mm^3, double-sided mechanically and electrochemically polished to a high optical quality, and recrystallized at 2073 K for 1 h. The typical grain size was in the range 20-100 μm (see below).

To simulate neutron irradiation, two specimens were irradiated with 20 MeV W ions to displacement damage of 0.3 and 3 displacements per atom (dpa) at the damage peak situated at a depth of 1.35 μm. The calculated depth damage profiles are shown in Fig. 1. The details of calculation can be found in [7]. The back side of specimens remained undamaged and was used as a reference surface for sputtering by Ar ions for simulation of sputtering by charge exchange atoms (CXA).

Prior sputtering by Ar ions starts, both sides of tungsten specimens were cleaned by exposing to deuterium and argon electron cyclotron resonance plasmas initiated by 2.35 GHz microwave source [4]. The rear side was cleaned in deuterium plasma with applying an accelerating voltage -60 V to the specimens' holder (D ion fluence was ~1.8×10^{23} ion/m^2), whereas the front side (preliminary irradiated with 20 MeV W ions) was cleaned in argon plasma with accelerating voltage -200 V (Ar ion fluence was ~2.1×10^{22} ion/m^2). Similar treatment was usually used to remove organic contaminants from the surface, and the reflectance measured after such a procedure, was accepted as an initial value.

Because the rate of sputtering of tungsten with hydrogen and deuterium ions is very low, Ar ions with energy 600 eV were used to shorten the time of experiment. The same setup as for cleaning but with higher negative bias of 600 V was used for sputtering of the specimen fixed on

the water-cooled specimen holder. Both sides of each specimen were sputtered by 600 eV Ar ions sequentially in 7 steps. Total Ar ion fluences after each step are F1 = 2.3×10^{22} ion/m^2, F2 = 5.65×10^{22} ion/m^2, F3 = 1.2×10^{23} ion/m^2, F4 = 2.9×10^{23} ion/m^2, F5 = 4.4×10^{23} ion/m^2, F6 = 5.2×10^{23} ion/m^2, and F7 = 6.5×10^{23} ion/m^2. After cleaning and each sputtering step, the surface modification of the specimen was analyzed via optical microscopy and interferometry. Furthermore, the mass loss and optical characteristics were measured after each exposure step. Thus, the reflectance at several wavelengths was found as function of sputtered layer thickness. In total, the specimens were eroded to the depth ~3.9 μm. This depth exceeds the W-ion-induced damage zone, which does not exceed ~2.2 μm (Fig. 1).

The optical investigations included direct measurements of specular reflectance $R(\lambda)$ at normal light incidence within 220÷650 nm spectral range [4] and measurements of ellipsometric parameters (Ψ and Δ) within 450÷760 nm spectral range [8]. To investigate optical constants multi-angle ellipsometry was used [9] due to its sensitivity to surface structure modifications. The dependence on the probing light incidence angle θ of values of phase shift Δ between p- and s-components of the light and restored linear polarization azimuth Ψ were measured using laser (λ=632.8 nm) null-ellipsometer LEPh-3M-1. By the use of the obtained dependences $\Delta(\theta)$ and $\Psi(\theta)$, refractive index n and extinction coefficient k of the studied surfaces as well as the reflectivity at normal incidence R were calculated [10].

Micro-images of the specimen surface were obtained using optical microscopes MMI-2 (small magnification) and MII-4 (large magnification). Micro-interferometric setup [11] was used to investigate the specimen surface relief.

After applying the highest fluence (i.e., after termination of sputtering procedures) the specimens' surfaces were additionally analyzed by confocal laser scanning microscope (CLSM; Olympus LEXT OSL4000) for obtaining height maps and by Electron Backscatter Diffraction (EBSD; HKL/Oxford Nordlys II-detector and Channel 5 analysis software) implemented in a scanning electron microscope (SEM; FEI HELIOS NanoLab 600) for grain orientation determination. Exactly the same surface area was investigated with both techniques.

3. Experimental results

3.1. Optical microscopy, interferometry, and mass loss

Figs. 2a-f show interference patterns of both W-ion damaged and undamaged sides of the specimen after cleaning and sputtering by Ar ions. As is seen, the grain size is ~10÷100 μm, and the damaged with W^{6+} ions (left column) and undamaged surfaces (right column) are absolutely smooth: the interference fringes do not have any curving or distortion either on the grain boundaries or within grains. Similar results are evident from SEM photo images (not shown).

After cleaning, both sides of the specimens were sputtered by 600 eV Ar ions in a number of steps with gradual ion fluence increase (F1→F7). For each sample, the rear side was firstly sputtered then the specimen was turned over and the preliminary damaged side (0.3 and 3 dpa) was sputtered under the same conditions. Since the major results turned out to be independent upon the damage lever (0.3 and 3 dpa), all results shown below correspond to the 3 dpa dose only. Studies of the surface condition and optical properties were carried out after each sputtering procedure. The total fluence of Ar ions reached F7=$6.5 \cdot 10^{23}$ ions/m^2.

Figs. 2(a-f) demonstrate modification of interference patterns after certain sputtering procedures. One can see sharp shifts of interference fringes on boundaries of some grains (marked by arrows in Fig. 2c,e,f). Fringes' shifts indicate development of the stepped structure of the surface, what is typical for polycrystalline materials exposed to long-term sputtering [4]. This effect is related to a difference in sputtering yields of grains with different orientations [12]. Meanwhile inside each grain interference fringes remain parallel that means that the grains surface maintains its smoothness. Also one can see that such modifications are similar for both sides of the specimen (non-irradiated side (Figs. 2c,e) and the one preliminary irradiated with tungsten ions to 3 dpa dose (Fig. 2d,f)). Interferograms processing after each sputtering allowed determining the dependence of adjacent grains level difference Δh upon the ion fluence.

Fig. 3 shows the dependence of maximal measured Δh and the mass loss Δm on ion fluence. One can see that the difference in levels increases with increasing ion fluence. For the highest applied fluence the level of these grains turned out 0.95 μm lower that the level of the adjacent grains. This is about 25% of the average sputtered layer thickness (~3.9 μm). Meanwhile many grains have close values of sputtering yield, so the steps height remains hardly exceeding the sensitivity threshold of interferometry (~0.07 μm).

Average thickness of the sputtered layer, determined from the specimen mass loss after each sputtering step, growth linearly with the ion fluence (dotted line and solid circles at Fig. 3), and in the limit of accuracy of measurements does not depend on whether the specimen has been irradiated with high-energy W ions (circles) or not (dotted line). Similarly, there was no difference for specimen irradiated to the damage level of 0.3 dpa.

3.2. CLSM and SEM with EBSD analyses

Fig. 4 shows two surface areas of the size 0.64×0.64 mm^2 with the scale indicating steps between different grains. The largest steps ($\Delta z \approx 1.5$ μm) do significantly exceed the maximal step measured by an interferometer microscope ($\Delta h \approx 0.95$ μm, Fig. 2f). This could be explained by the limited statistics in the case of interferometry, i.e., the largest shift of interference bands just was not fell in the field of microscope.

The right upper part of Fig. 4b with the area around the grain with about (111) orientation (~9º deviation from the [111] direction) was analyzed in more details, as it is demonstrated in Fig. 5. This grain dominates over all neighboring grains with Δz varying between 0.4 and 1.3 μm. According to EBSD data (not shown), all these neighboring grains have orientations that are strongly different from the eminent one. However, alongside with such big step heights between grains having strongly different orientations, there are many small step heights of less than 100 nm (down to 20 nm) observed between adjoining grains with only small orientation difference.

In Fig. 6, the scaled histograms of the height, i.e., probability density functions PDF, of the two CLSM data shown in Fig. 4 are given. The standard deviation of the mean height (after leveling) is for both data sets 0.39. The height zero point is defined by dividing the area of the PDF into half, i.e., defining mean erosion level which was 3.9 μm (from mass loss data). The width of the distribution determines the maximal step which could be observed. As it is evident from Fig. 6, all grains with (111) or close orientations exhibit low sputtering yields; (110) has a higher yield, and (100) grains exhibit a yield in the middle. Remarkable is the asymmetry of the distribution. It is not clear if the observed texture resulting in a higher amount of grains close to (110) and a lower amount of grains close to (111) is sufficient to explain this asymmetry.

3.3. Optical characteristics

3.3.1. Reflectivity at normal incidence angle

Figs. 7a,b show the evolution of spectral reflectivity at normal incidence of the non-irradiated (0 dpa) and irradiated (3 dpa) sides of the specimen just after cleaning and after two sputtering stages. One can see that reflectivity spectra of the specimen are in good agreement with reference data [13]. It is also obvious that reflectivity at normal incidence is not significantly affected by surface modification induced by 600 eV Ar ions sputtering either for non-irradiated surface or for the surface that was preliminary irradiated with tungsten ions.

3.3.2. Ellipsometry

Figs. 8(a-d) present angular dependences (the angle θ is reading from the normal to surface, wavelength λ=632.8 nm) of ellipsometric parameters Ψ and Δ after cleaning, the intermediate and the last sputtering procedures for non-irradiated side (0 dpa) and for the side preliminary irradiated (3 dpa) with tungsten ions. As one can see, the sputtering procedure affected neither quality nor quantity on the ellipsometric parameters angular dependences; correspondingly the principle angle $\theta_p=78^\circ$ (the angle when Δ=90º) is not affected as well. It means that the sputtering revealed no modified layer on the surface, which remains bare.

Ellipsometric parameters Ψ and Δ spectra after cleaning and after the same sputtering steps

as in Fig. 8 are shown in Fig. 9. One can see that Ψ does not change. It is an expected result since the ion sputtering does not bring about the formation of significant roughness of the in-grain surfaces. Meanwhile Δ changes slightly and for the surface preliminary irradiated with tungsten ions these changes are a bit greater.

Fig. 10 shows refractive index *n* and extinction coefficient *k* as well as specular reflectance $R(\lambda)$ calculated from experimental data (Fig. 8). For the better interpretation of the ellipsometer data, a number of the models of the surface were checked. It was ascertained that the model of bare surface is still the optimal one. This model is adequate since sputtering revealed no modified layer on the surface. It is clear from Fig. 10 that main optical parameters are not affected by sputtering. The results of $R(\lambda)$ dependences are qualitatively similar to the ones obtained by direct measurements at normal incidence (Fig. 7). The quantitative difference between calculated and measured values of reflectivity, about several percents, is because these methods (ellipsometry and reflectometry) are based on different physical phenomena [14]: ellipsometry "sees" only the surface parts with specular reflection. Reflectometry reflects the integral energy of reflected light. At last case every defect of the surface increases the diffuse component and decreases the specular reflection.

4. Discussion and conclusions

It has been shown in this study that recrystallized W mirror specimens preliminary damaged with W ions up to a damage level of 3 dpa that is typical for ITER, behave under sputtering with 600 eV Ar ions identically to the undamaged specimens. Concerning FM operating conditions in ITER it means that the results of neutrons and CXA mutual impact on tungsten FM will be similar to the impact of CXA only. Sputtering of ~3.9 μm layer resulted in ~2% change of reflectivity at normal incidence within the whole studied spectral range. It is surprising but in this meaning the behavior of recrystallized tungsten mirrors is rather similar to behavior of monocrystalline mirrors studied earlier [4]. The reason of this fact is probably the absence of in-grain relief and normal incidence of light.

The second result is important for erosion of tungsten in ITER: with good reason we may state that neutrons will not change noticeably the rate of erosion under plasma impact of the W protective tiles.

According to ellipsometry, recrystallized tungsten surface preliminary damaged with 20 MeV W ions and bombarded with argon ions has no layer that would significantly modify optical properties of diagnostic mirrors.

Important difference was found in the sputtering rates of differently oriented grains in tungsten as compared with stainless steel mirror specimens [12]. These metals belong to bcc and

fcc metals, correspondingly. In the case of stainless steel the highest sputtering rate was found for the face (111) [12], which is the densest face. In the case of tungsten this face, in contrast, is the most resistant to sputtering, but the face (110), which is densest for bcc metals, showed the highest sputtering yield. As follows from results of interferometry, CLSM, and EBSD measurements of heights between neighboring grains, the difference in sputtering yields for (111) and (110) reaches as much as tens of percents.

In conclusion, it should be mentioned the principal difference of our experiments modeling simultaneous impact of neutrons and CXA with the experiments reported by the authors of [15, 16], where the impact of neutrons was simulated by irradiation of W specimens with 3.5-4 MeV α-particles. In our case there is no change of the composition of the near-surface layer due to helium accumulation. As for the non-effect of preliminary damaging on sputtering rate with plasma ions, our results are in a good qualitative agreement with data published in [15, 16].

In this study Ar ions were used for sputtering, thus the conclusions should be applied to ITER conditions cautiously. To make reactor conditions imitation more realistic we intend to carry out similar experiments with specimens irradiated with 20 MeV W ions up to higher doses and sputter them by deuterium plasma with wide ion energy distribution, qualitatively similar to energy distribution of CXA (e.g. [17]).

Table 1. The ratio of the reflectance **R** at the indicated wavelengths to the sputtering yield **Y** (atoms/ion) for selected metals sputtered by 300 eV D ions at normal incidence.

Metal	R / Y for three wavelengths		
	250 nm	500 nm	800 nm
Al	21	21	20
SS	19	34	36
Cu	7	12	18
Ag	7	24	25
Rh	93	110	117
Mo	246	286	233
W	6125	6125	6125

References

1. V.S. Voitsenya, V.G. Konovalov, A.F. Shtan', et al. Some problems of the material choice for the first mirrors of plasma diagnostics in a fusion reactor. Rev. Sci. Instrum. **70** (1999) 790.
2. V.S. Voitsenya, A.F. Bardamid, Yu. Borisenko, et al. Imitation of a fusion reactor environment on optical properties of metallic mirrors. J. Nucl. Mater., **233–237** (1996) 1239.
3. G. Federici, C.H. Skinner, J.N. Brooks, et al. Plasma–material interaction in current tokamaks and their implications. Nucl. Fusion, **41** (2001) 1967.
4. D. Orlinski, V. Voitsenya and K. Vukolov. First mirrors for diagnostic systems of an experimental fusion reactor. I. Simulation mirror tests under neutron and ion bombardment. Plasma Devices Opers. **15**, Issue 1 (2007) pp. 33–75.
5. W.M. Shu, G.-N. Luo, T. Yamanishi. Mechanisms of retention and blistering in near-surface region of tungsten exposed to high flux deuterium plasmas of tens of eV. J. Nucl. Mater. **367–370** (2007) 1463-1467.
6. S. Lindig, M Balden, V Kh Alimov, T Yamanishi, WM Shu, J Roth. Subsurface morphology changes due to deuterium bombardment of tungsten. Phys. Scr. **T138** (2009) 014040 (5 pp).
7. B. Tyburska, V.Kh. Alimov, O.V. Ogorodnikova, K. Schmid, K. Ertl. Deuterium retention in self-damaged tungsten. J. Nucl. Mater. **395** (2009) 150–155.
8. A.I. Belyaeva, A.A. Galuza, V.F. Klepikov et al. Problems of Atomic Science and Technology 2009, V.93, №2, pp. 191-197 (in Russian).
9. A.A. Galuza, K.A. Slatin, A.I. Belyaeva et al. Instr. and Exper. Techn. **46 (**2003) 477.
10. Fujiwara H. Spectroscopic ellipsometry: principles & applications. Chichester: John Wiley & Sons, 2007, 370 p.
11. A.I. Belyaeva, A.A. Galuza, A.D. Kudlenko. Pribory i Technika Exper. 2008, 135 (in Russian).
12. M. Balden, A.F. Bardamid, A.I. Belyaeva et al. J. Nucl. Mater. **329-333** (2004) 1515-1519.
13. Palik E.D. (Ed.) Handbook of Optical Constants of Solids. San Diego: Acad. Press, 1991.
14. A.I. Belyaeva, V.Kh. Alimov, A.A. Galuza et al. Optical characteristics of recrystallized tungsten mirrors exposed to low-energy, high flux D plasmas. J. Nucl. Mater. **413** (2011) 5-10.
15. V.S. Koidan, B.I. Khripunov, A.I. Ryazanov, A.N. Brukhanov, O.K. Chugunov, V.M. Gureev, S.N. Kornienko, B.V. Kuteev, S.T. Latushkin, V.B. Petrov, E.V. Semenov, V.G. Stolyarova, V.N. Unezhev, L.S. Danelyan, V.S. Kulikauskas, V.V. Zatekin. Effects of Plasma Interaction with Radiation-Damaged Tungsten. Paper FTP/3-3Rb presented at 23rd IAEA Fusion Energy Conference, 11-16 October 2010, Daejon, Rep. Korea. http://www-pub.iaea.org/mtcd/meetings/cn180_papers.asp.
16. B.I. Khripunov, A.N. Brukhanov, V.M. Gureev, V.S. Koidan, S.N. Kornienko, S.T. Latushkin, V.B. Petrov, A.I. Ryazanov, E.V. Semenov, V.G. Stolyarova, V.N. Unezhev, L.S. Danelyan, V.S. Kulikauskas, V.V. Zatekin, V.G. Vostrikov, E.A. Romanovsky. Plasma effect on tungsten damaged by high-energy alpha particles: Erosion and deuterium trapping. J. Nucl. Mater. **415** (2011) S649–S652.
17. R. Behrisch, G. Federichi, A. Kukushkin, *et al.* Material erosion at the vessel walls of future fusion devices. J. Nucl. Mater., **313**–**316** (2003) 388.

Figure captions

Fig. 1. Depth distributions of dpa in the near-surface layer calculated for W target exposed to 20 MeV tungsten ions with fluence $4.5 \cdot 10^{18}$ ions/m^2 (upper curve) and $4.5 \cdot 10^{17}$ ions/m^2 (lower curve).

Fig. 2. Interference patterns on the surface of recrystallized W specimen. Non-irradiated side: a, c, e; irradiated side (3 dpa): b, d, f. After cleaning and Ar ion fluence: F1=$2.3 \cdot 10^{22}$ ions/m^2 (a, b); F5=$4.35 \cdot 10^{23}$ ions/m^2 (c, d); F7=$6.45 \cdot 10^{23}$ ions/m^2 (e, f). The arrows indicate sharp shifts of interference fringes in boundaries of grains.

Fig. 3. Dependence of relative height shift Δh of adjoining grains for 3 dpa rcW specimen on Ar ion fluence as seen in the interferometer microscope (squares). Mass loss of W specimens depending on the fluence of Ar plasma ions is shown for comparison (full circles for 3 dpa and dotted line for 0 dpa).

Fig. 4. CLSM data for two surface areas of the 3.0 dpa specimen surface after exposure to the highest fluence F7=$6.45 \cdot 10^{23}$ ions/m^2 (Image size: 0.64x0.64 mm^2). The details for area in the upper right part of the Fig.4b image are shown in Fig.5.

Fig. 5. 2D (a) and 3D (b) images (129x129 μm^2) obtained with CLSM of the part of surface area in Fig. 4b around the grain with about (111) orientation (~9º deviation from the [111] direction). The specimen irradiated to 3 dpa after Ar ion fluence $6.45 \cdot 10^{23}$ ions/m^2.

Fig. 6. The probability density functions PDF of the two CLSM data shown in Fig. 4 for rc W specimen irradiated to 3 dpa and sputtered by Ar^+ ions to the mean depth 3.9 μm (ion fluence $6.45 \cdot 10^{23}$ ions/m^2).

Fig. 7. Reflectivity spectra of non-irradiated (a) and irradiated (b) sides of rc W (3 dpa) mirror specimen after: cleaning, Ar ion fluences F1=$2.3 \cdot 10^{22}$ ions/m^2, and F7=$6.5 \cdot 10^{23}$ ions/m^2.

Fig. 8. Angular dependences of ellipsometric parameters Ψ(a, b) and Δ(c, d) for non-irradiated (0 dpa) and irradiated (3 dpa) sides of the rc W specimen, after cleaning and two ion fluence steps: F1=$2.3 \cdot 10^{22}$ ion/m^2 and F7=$6.45 \cdot 10^{23}$ ions/m^2.

Fig. 9. Ellipsometric parameters Ψ (a, b) and Δ (c, d) spectra for non-irradiated (0 dpa) and irradiated sides (3 dpa) of the rc W specimen after cleaning and two ion fluence steps: F1=$2.3 \cdot 10^{22}$ ion/m^2 and F7=$6.45 \cdot 10^{23}$ ions/m^2.

Fig. 10. Optical constants (n and k) and reflectivity (R) spectra after cleaning, the first and the last sputtering with Ar plasma ions: non-irradiated side (a, c, e) and the irradiated one (b, d, f). For comparison n, k and R spectra of tungsten by E.D. Palik [13] are shown.

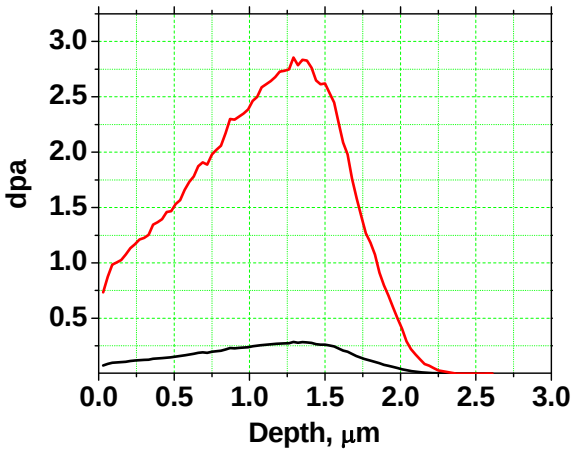

Fig. 1. Depth distributions of dpa in the near-surface layer calculated for W target exposed to 20 MeV tungsten ions with fluence $4.5 \cdot 10^{18}$ ions/m^2 (upper curve) and $4.5 \cdot 10^{17}$ ions/m^2 (lower curve).

.

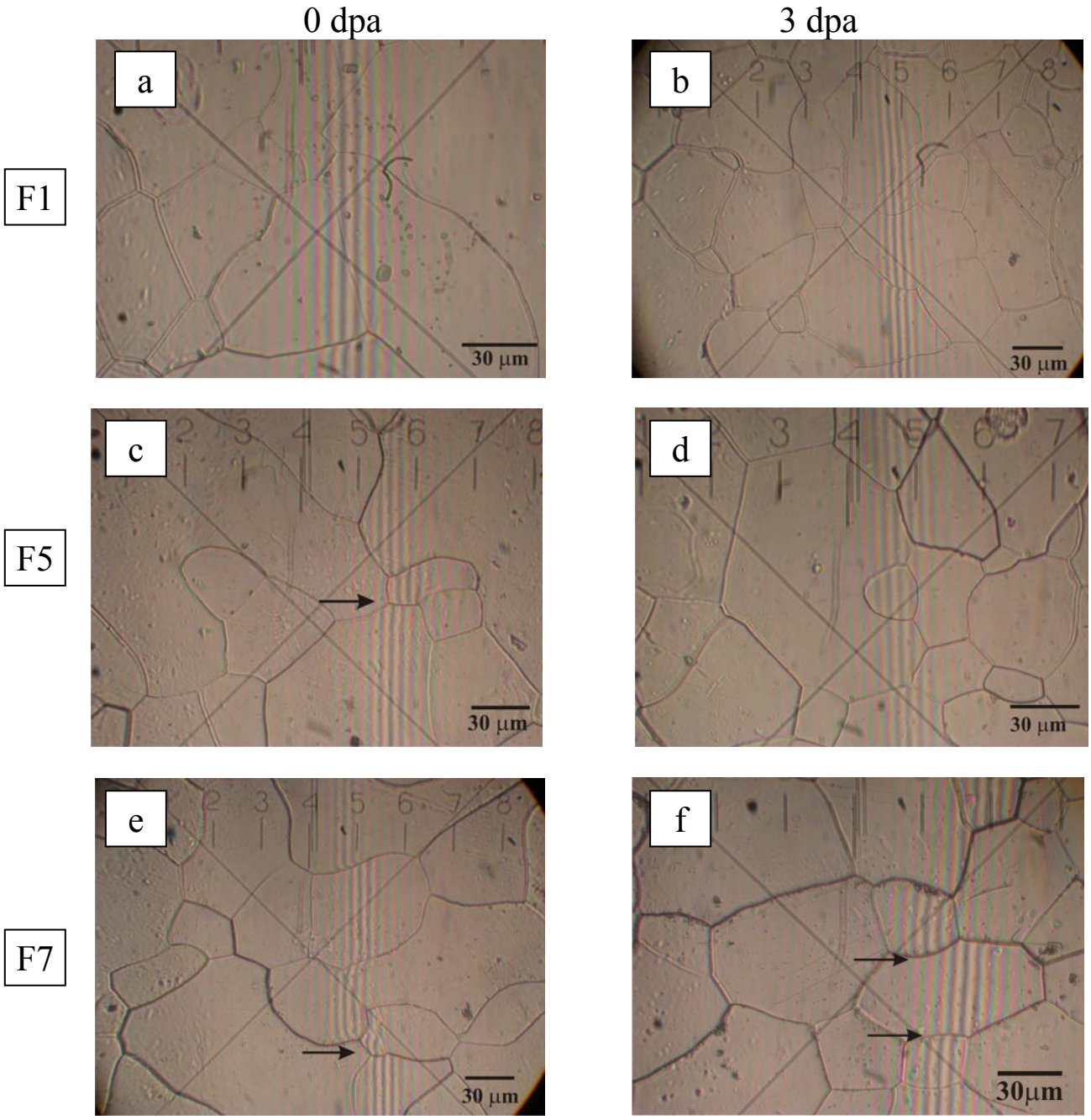

Fig. 2. Interference patterns on the surface of recrystallized W specimen. Non-irradiated side: a, c, e; irradiated side (3 dpa): b, d, f. After cleaning and Ar ion fluence: F1=$2.3 \cdot 10^{22}$ ions/m^2 (a, b); F5=$4.35 \cdot 10^{23}$ ions/m^2 (c, d); F7=$6.45 \cdot 10^{23}$ ions/m^2 (e, f). The arrows indicate sharp shifts of interference fringes in boundaries of grains.

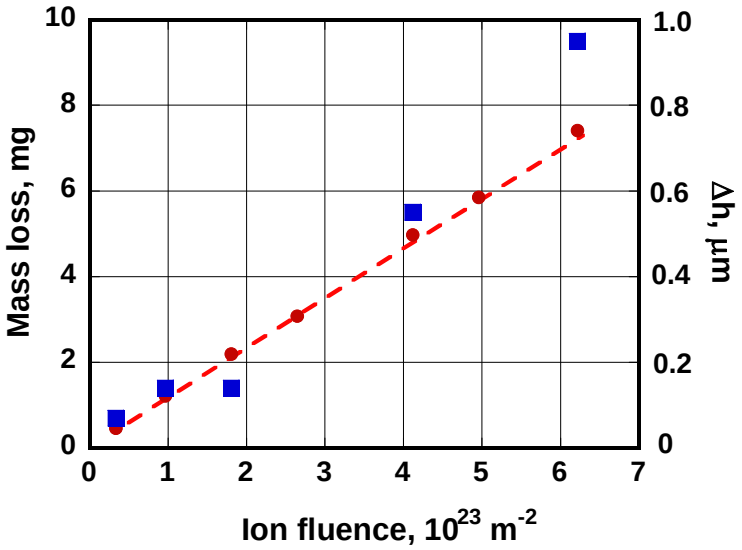

Fig. 3. Dependence of relative height shift Δh of adjoining grains for 3 dpa rcW specimen on Ar ion fluence as seen in the interferometer microscope (squares). Mass loss of W specimens depending on the fluence of Ar plasma ions is shown for comparison (full circles for 3 dpa and dotted line for 0 dpa).

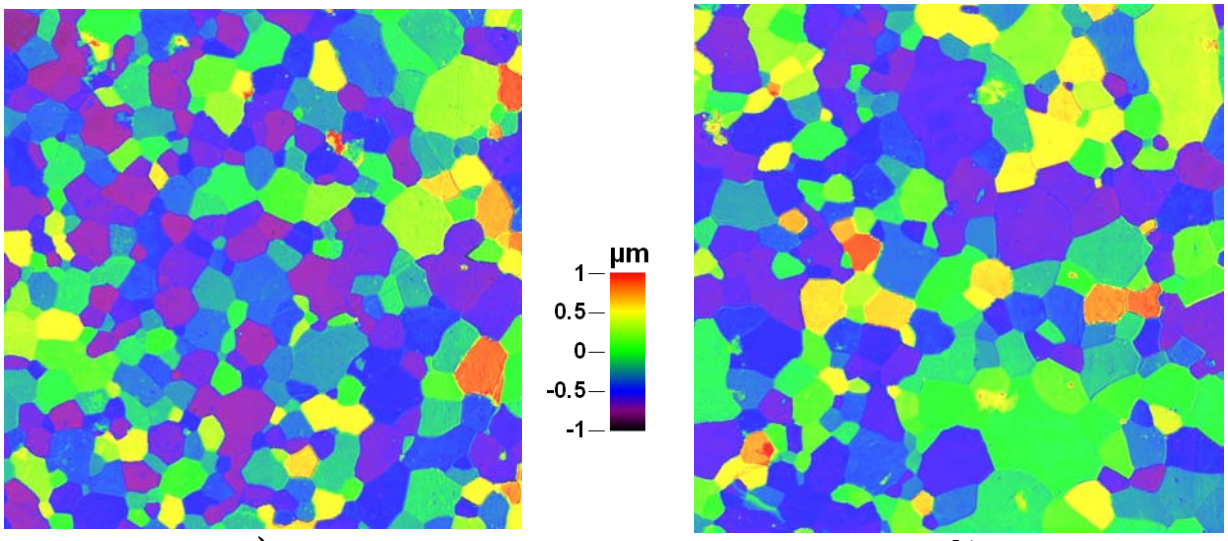

a) **b)**

Fig. 4. CLSM data for two surface areas of the 3.0 dpa specimen surface after exposure to the highest fluence F7=$6.45 \cdot 10^{23}$ ions/m^2 (Image size: 0.64x0.64 mm^2). The details for area in the upper right part of the Fig.4b image are shown in Fig.5.

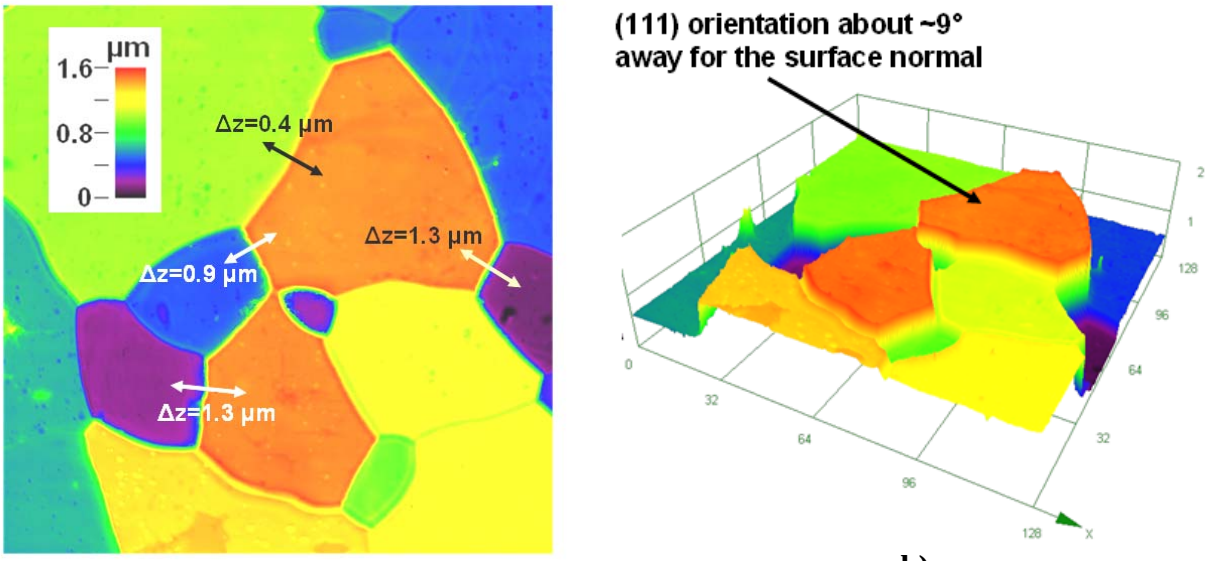

a) **b)**

Fig. 5. 2D (a) and 3D (b) images (129x129 μm^2) obtained with CLSM of the part of surface area in Fig. 4b around the grain with about (111) orientation (~9º deviation from the [111] direction). The specimen irradiated to 3 dpa after Ar ion fluence $6.45 \cdot 10^{23}$ ions/m^2.

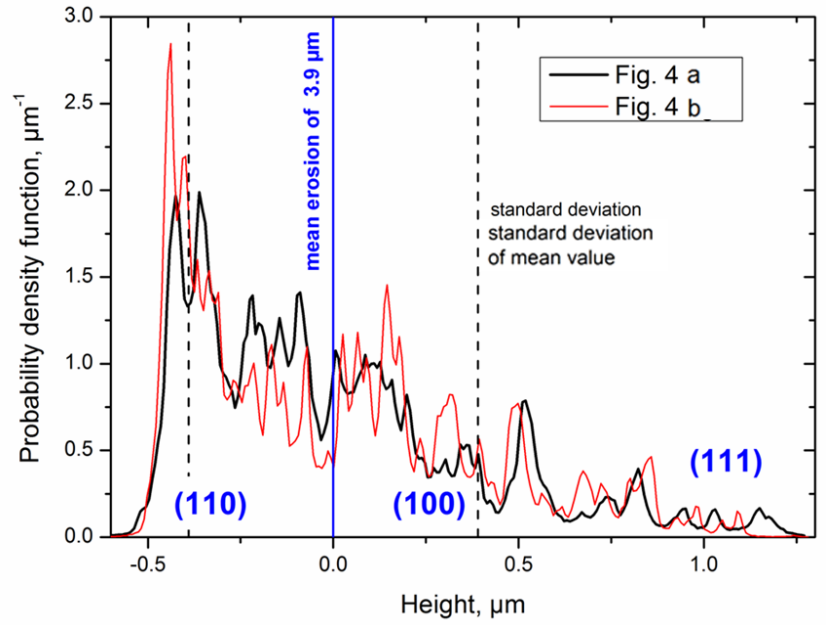

Fig. 6. The probability density functions PDF of the two CLSM data shown in Fig. 4 for rc W specimen irradiated to 3 dpa and sputtered by Ar^+ ions to the mean depth 3.9 µm (ion fluence F7=$6.45 \cdot 10^{23}$ ions/m^2).

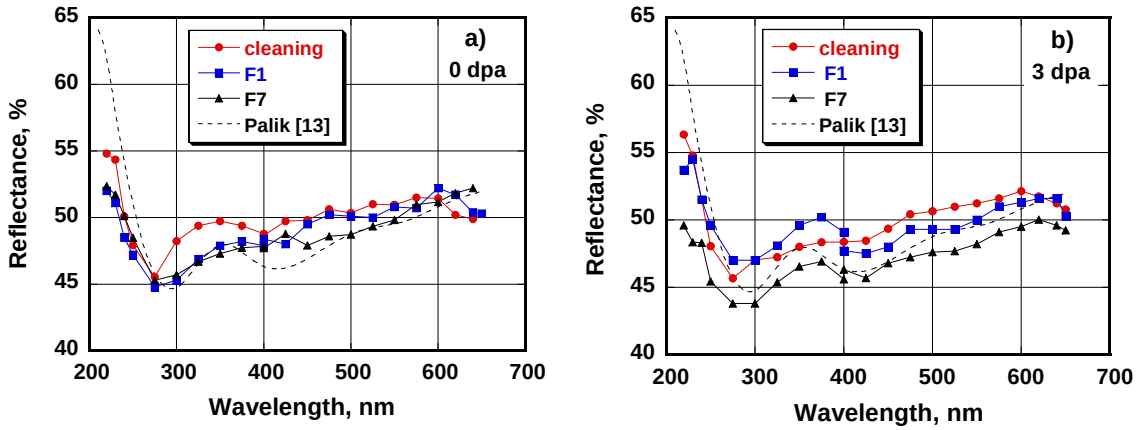

Fig. 7. Reflectivity spectra of non-irradiated (a) and irradiated (b) sides of rc W (3 dpa) mirror specimen after: cleaning, Ar ion fluences F1=$2.3 \cdot 10^{22}$ ions/m^2, and F7=$6.45 \cdot 10^{23}$ ions/m^2.

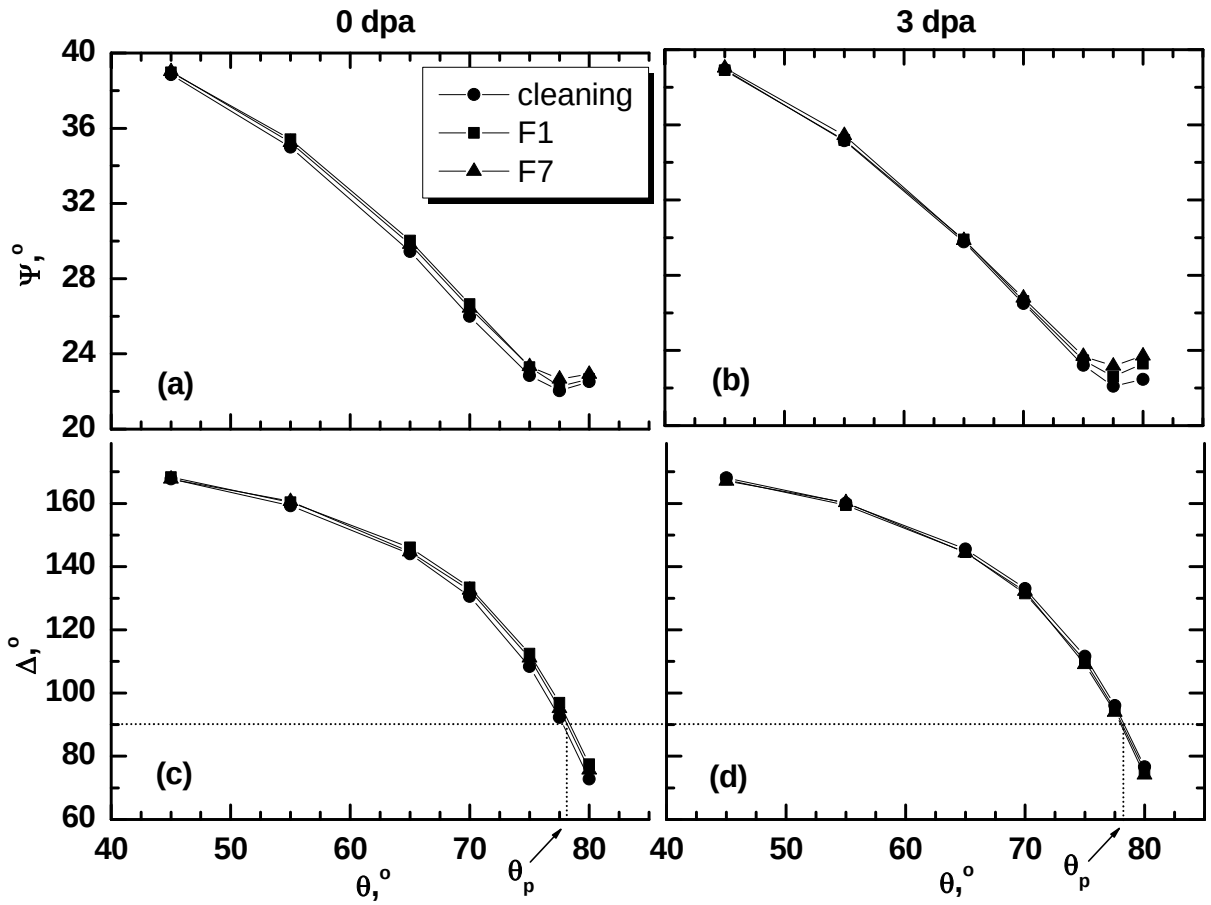

Fig. 8. Angular dependences of ellipsometric parameters Ψ(a, b) and Δ(c, d) for non-irradiated (0 dpa) and irradiated (3 dpa) sides of the rc W specimen, after cleaning and two ion fluence steps: F1=$2.3 \cdot 10^{22}$ ions/m^2 and F7=$6.45 \cdot 10^{23}$ ions/m^2.

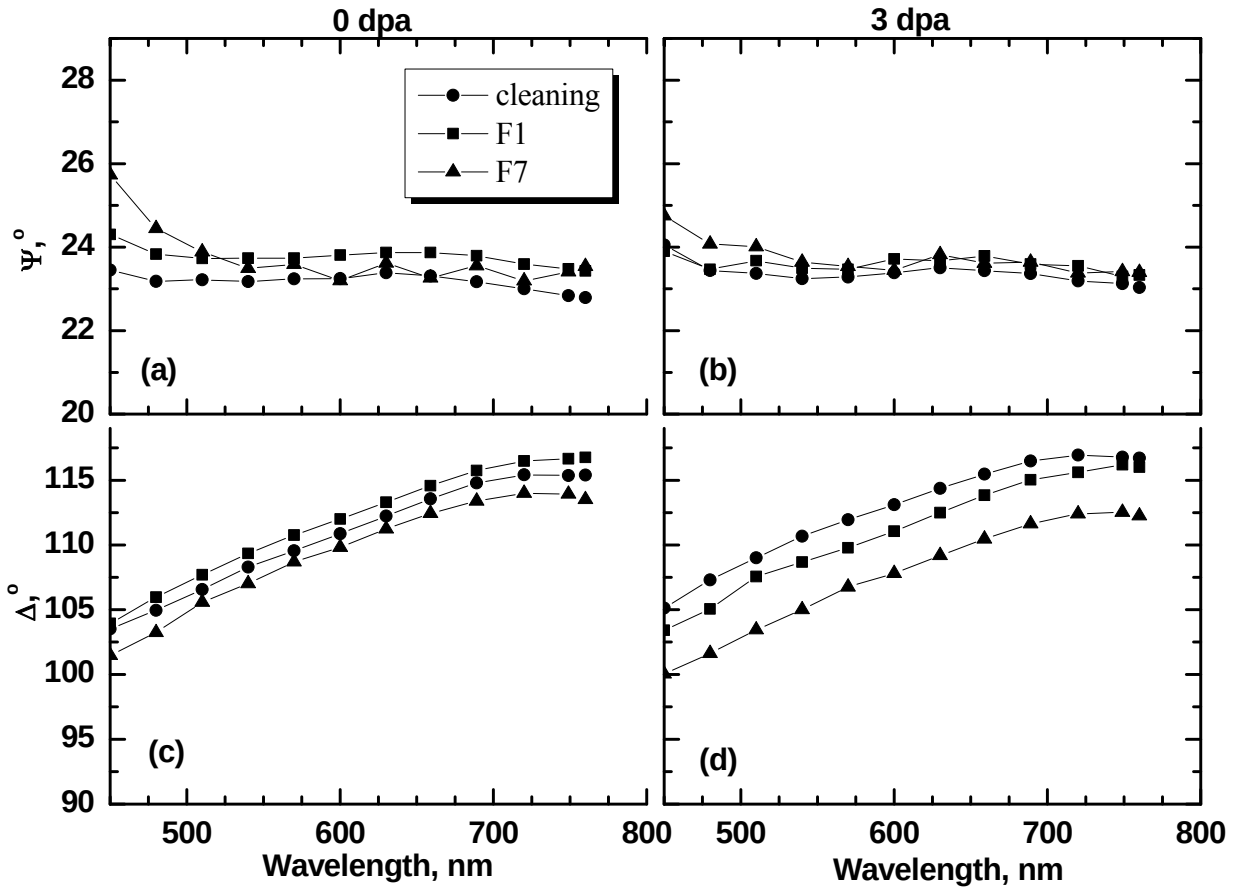

Fig. 9. Ellipsometric parameters Ψ (a, b) and Δ (c, d) spectra for non-irradiated (0 dpa) and irradiated sides (3 dpa) of the rc W specimen after cleaning and two ion fluence steps: F1=$2.3 \cdot 10^{22}$ ions/m^2 and F7=$6.45 \cdot 10^{23}$ ions/m^2.

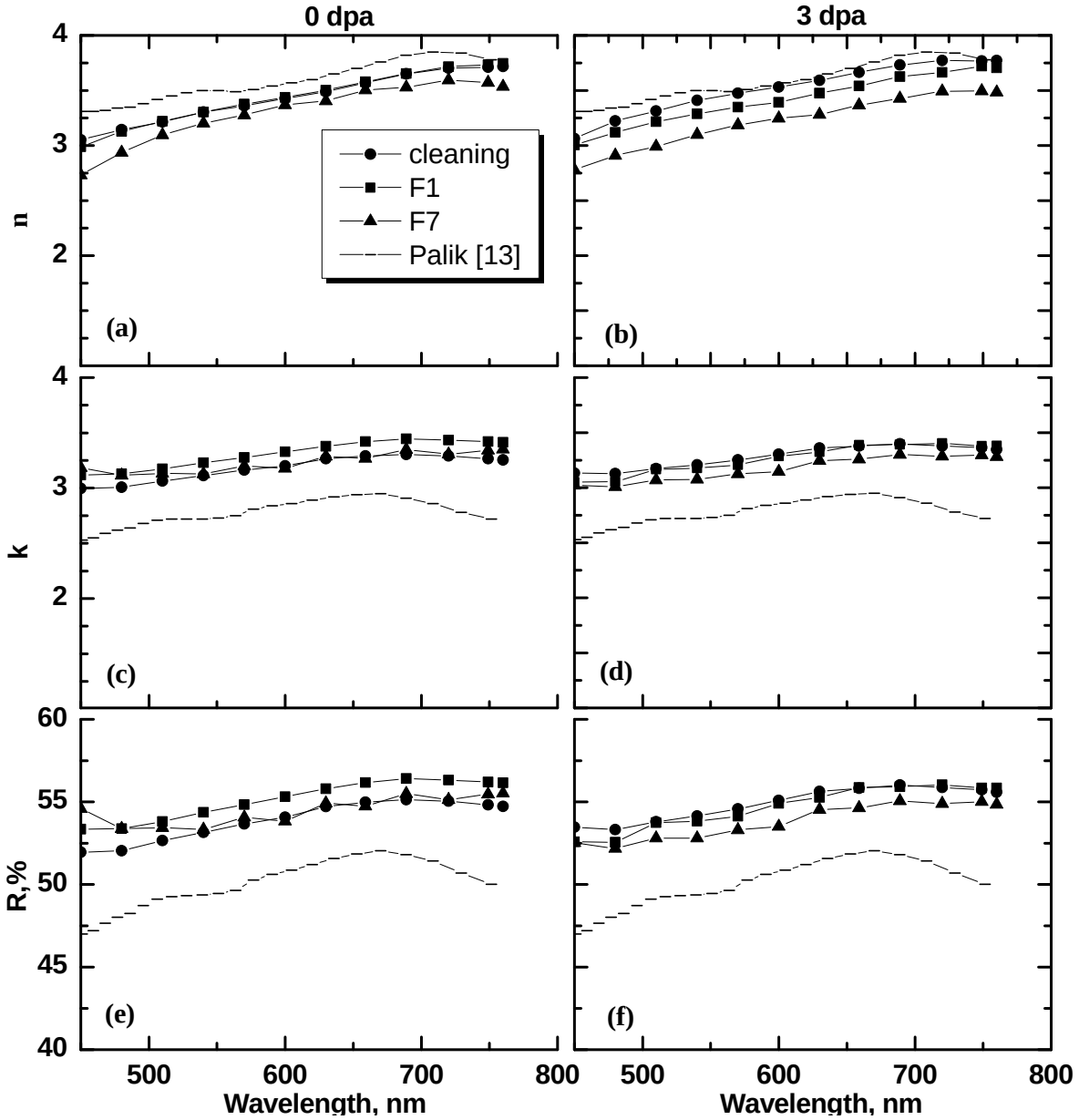

Fig. 10. Optical constants (n and k) and reflectivity (R) spectra after cleaning, the first and the last sputtering with Ar plasma ions: non-irradiated side (a, c, e) and the irradiated one (b, d, f). For comparison n, k and R spectra of tungsten by E.D. Palik [13] are shown.

Table 1. The ratio of the reflectance **R** at indicated wavelengths to the sputtering yield **Y** at normal incidence (atoms/atom) with 0.3 keV deuterium ions for some metals [4].

Metal	R / Y for three wavelengths		
	250 nm	500 nm	800 nm
Al	21	21	20
SS	19	34	36
Cu	7	12	18
Ag	7	24	25
Rh	93	110	117
Mo	246	286	233
W	6125	6125	6125